frontiers in Materials

ORIGINAL RESEARCH
published: 06 December 2019
doi: 10.3389/fmats.2019.00318

Microstructure and Mechanical Properties of Ti-35Nb-2Ta-3Zr Alloy by Laser Quenching

Ting Zhang[1], Qing Fan[2], Xiaoli Ma[3], Wen Wang[1], Kuaishe Wang[1]*, Pingquan Shen[2] and Junlin Yang[2]*

[1] Xi'an University of Architecture and Technology, Xi'an, China, [2] Xinhua Hospital, Shanghai Jiao Tong University, Shanghai, China, [3] State Key Laboratory of Metal Matrix Composites, School of Material Science and Engineering, Shanghai Jiao Tong University, Shanghai, China

In this work, using laser quenching technology to modify the surface of β-Ti-35Nb-2Ta-3Zr alloy. The microstructure and deformation mechanism of laser-quenched region were analyzed in detail by using X-ray diffraction (XRD), scanning electron microscope (SEM), and transmission electron microscope (TEM). Dislocations and α″ martensite transformation occur during the process. The cyclic loading-unloading stress-strain curve is used to evaluate the superelasticity of the alloy. After laser quenching, the superelasticity and microhardness of the alloy increases, and the toughness decreases. Grain coarsening is also obtained during laser quenching.

Keywords: microstructure, mechanical properties, deformation mechanism, β titanium, laser quenching

OPEN ACCESS

Edited by:
Lai-Chang Zhang,
Edith Cowan University, Australia

Reviewed by:
Jiang Zheng,
Chongqing University, China
Lechun Xie,
Wuhan University of Technology, China
Gang Chen,
University of Science and Technology Beijing, China

***Correspondence:**
Qing Fan
fanqing@xinhuamed.com.cn
Kuaishe Wang
wangkuaishe888@126.com

Specialty section:
This article was submitted to Structural Materials, a section of the journal Frontiers in Materials

Received: *21 October 2019*
Accepted: *21 November 2019*
Published: *06 December 2019*

Citation:
Zhang T, Fan Q, Ma X, Wang W, Wang K, Shen P and Yang J (2019) Microstructure and Mechanical Properties of Ti-35Nb-2Ta-3Zr Alloy by Laser Quenching. Front. Mater. 6:318. doi: 10.3389/fmats.2019.00318

INTRODUCTION

β-titanium alloys have good biocompatibility, low modulus, non-toxicity, and excellent corrosion resistance, which are widely used in medical treatment, especially in dentistry and orthopedics (Saji et al., 2009; Wang et al., 2009a; Lin et al., 2013). The alloys show a variety of mechanical properties, which are related to their deformation mechanisms. In 2003, Saito (2003) reported the activation of dislocation-free plastic deformation mechanisms in β titanium alloys, obtaining super mechanical properties. This work had triggered a research wave on the deformation mechanisms of β-titanium alloys and their influence on mechanical properties. Recently, a variety of deformation mechanisms in β titanium alloys have been found, including stress-induced phase transformations ($\beta \rightarrow \alpha'$, $\beta \rightarrow \alpha''$ or $\beta \rightarrow \omega$) (Ozan et al., 2017; Wang et al., 2017; Lai et al., 2018; Maghsoudlou et al., 2018; Yang et al., 2018; Gao et al., 2019), {332} twinning (Tobe et al., 2014; Lai et al., 2016, 2018; Gao et al., 2019), {112} twinning (Yao et al., 2017; Gao et al., 2018), as well as dislocation slip (Lai et al., 2018; Gao et al., 2019). It was also revealed that the dislocation slip dominates the plastic deformation in the β-titanium alloys with higher stability, while reducing the stability of the β-titanium alloys activates other deformation mechanisms such as deformation twins and martensite transformation (Lai et al., 2016; Maghsoudlou et al., 2018). Generally, phase transformation, twins or dislocation slip can be activated individually or simultaneously, which strongly influence the mechanical properties during processing. For example, Gao et al. (2018) reported that a new Ti-7Mo-3Cr (wt.%) alloy with high yield strength about 695 MPa and strain hardening rate about 1,600–1,900 MPa, and the yield strength of the alloy phase with a separate twin system is much greater. which was attributed to the combined action of two twin systems of {112} <111> and {332} <113> twins, much better compared to alloys with a single twin system. Min et al. (2012) found that that the combination of twinning and slip in Ti–Mo-based alloys, can enhance the

uniform elongation and maintain high strength. In addition, it was reported that the stress-induced α" martensitic during cold rolling contributed to the spectacular work hardening behavior, resulting in super elastic and pseudo-elastic zones of the tensile stress-strain curves, and reduce the elastic shear modulus (Wang et al., 2008a, 2009b; Maghsoudlou et al., 2018).

Owing to the good matching of implants and bone tissue is as important as their mechanical properties, many scholars have used different techniques to modify the surface of β-titanium alloy, and also studied the deformation mechanisms during modification. Although the methods for surface modification of titanium alloy such as plasma spraying (Sathish et al., 2011), ion implantation (Vlcak et al., 2019), micro-arc oxidation (Chen et al., 2013; Liu et al., 2015), friction stir processing (FSP) (Wang et al., 2015, 2017; Ding et al., 2016, 2019), and shot peening (Xie et al., 2016) can effectively improve the biocompatibility and mechanical properties of the titanium alloy, but there are still various problems. For instances, the coatings prepared by plasma spraying have poor adhesion to the substrate and are easy to fall off, the films prepared by ion implantation and micro-arc oxidation are too thin for poor performance (Liu et al., 2004; Chouirfa et al., 2018; Zhang and Chen, 2019).

Laser processing is considered to be one of the most promising surface modification methods (Baker, 2010; Chen et al., 2018), mainly including laser cladding, laser remelting and laser quenching, which can form a good metallurgical bond between the reinforcement layer and the matrix, which had been obtained in the work of Man et al. (2001), Sun et al. (2003), and Guo et al. (2007). Moreover, Sun et al. (2003) found that the α phase has changed to needle-like a′ martensite after the laser surface remelting of pure titanium, and the martensite formed by rapid cooling of the laser surface remelting shows a hexagonal close-packed crystal structure with high hardness but relatively low ductility. However, a more detailed analysis of the phase transition mechanism during the processing has not occurred. As for laser quenching titanium alloys, previous studies are only about the effect of fretting wear and sliding friction characteristics after laser quenching of TC11 titanium alloy (Dai et al., 1997), the effect of laser quenching on the microstructure and mechanical properties of β-titanium alloys have not been reported.

In this work, the Ti-35Nb-2Ta-3Zr β titanium alloy was prepared by the vacuum consumable smelting technique and laser quenching technology. A cyclic tensile test was used to assess the superelasticity of the material. The microstructural evolution of laser-quenched Ti-35Nb-2Ta-3Zr alloy was studied in this paper, and the deformation mechanism and its influence on superelastic behavior during laser quenching were also studied.

EXPERIMENTAL

Material Preparation

The Ti-Nb-Ta-Zr alloy with a nominal composition of Ti-35Nb-2Ta-3Zr (wt.%) was prepared by the vacuum consumable smelting technique. The mass fraction of each element of the prepared material was determined by hydrometallurgical chemical composition analysis, as shown in **Table 1**.

TABLE 1 | Chemical composition (wt.%) of the Ti-35Nb-2Ta-3Zr alloys.

Nb	Ta	Zr	Ti
34.60	2.70	3.04	Bal.

Ingot of Ti-35Nb-2Ta-3Zr alloy was prepared by a vacuum consumable electric arc furnace. The ingot was hot forged at 950°C to remove the scale on the surface of the material, and then annealed at the same temperature for 3–5 min.

Laser Quenching

The laser quenching was conducted on a laser material processing system mainly equipped with a 3.5 kW ROFIN DL 035Q semiconductor laser, Fanuc trajectory planning and control robot, and coaxial focus powder feeding system, as shown in **Figure 1A**. In this research, the semiconductor laser with an output laser wavelength of 808–940 nm. The laser quenching process were conducted in argon protective atmosphere. **Figure 1B** shows the basic schematic of a semiconductor laser nozzle.

After annealing, the surface of the alloy was polished to remove scale, straightened, then washed with acetone, and fixed on the working table of the semiconductor laser device. With the treated surface facing up, the alloy was subjected to laser quenching under argon protection, and the processing pass was 1 pass. The laser power was 500 W and the scanning speed was 12 mm/s.

Microstructural Characterization

After laser treatment, the samples were sectioned, mounted, coarsely ground, finely ground, coarsely polished, finely polished, and then etched by Keller's reagent (1 vol% HF, 1 vol% HNO_3, 1 vol% HCl in water) and for a Zeiss Imager.Optical microscope (OM) and a JEOL-JSM7600F scanning electron microscope (SEM) investigation. Phase analysis was carried out with X-ray diffraction (XRD) and transmission electron microscope (TEM) and the microstructure evolution of the materials after laser quenching were observed. XRD analysis was performed using a Cu Kα radiation source, which with an accelerating voltage of 40 kV and a current of 250 mA. TEM analysis was performed in a JEOL-JEM2100F microscope operated at 200 kV. Vickers microhardness measurements were performed on a Zwick/Roell JS-2000 microhardness tester using a 200 g load for a dwell time of 15 s.

Cycle Tensile Testing

To evaluate the tensile properties of Ti-35Nb-2Ta-3Zr alloy, some samples were used for cyclic tensile tests. The tensile tests were carried out at a strain rate of 1.0×10^{-4} s^{-1}. The cyclic tensile strain during loading-unloading testing was 1, 2, 3, 4%, respectively. The specimens had the gauge length of 20 mm, width of 5 mm, and thickness of 3 mm.

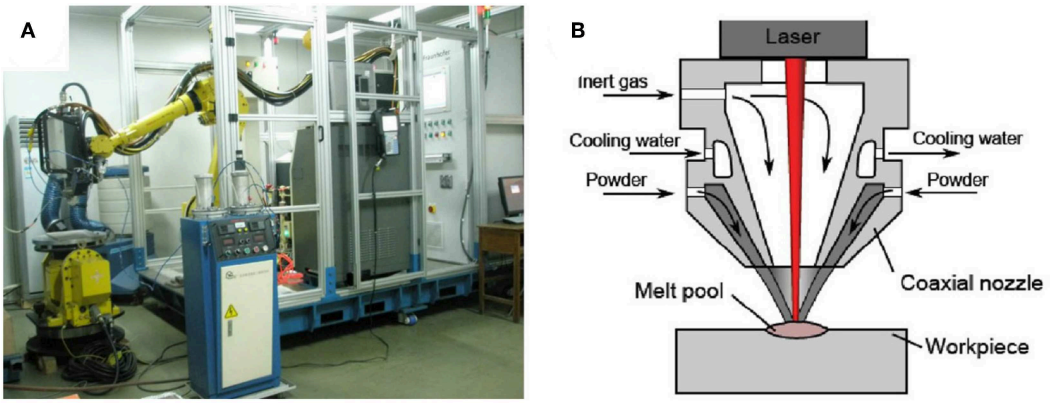

FIGURE 1 | (A) The laser treatment system, **(B)** schematic diagram of semiconductor laser nozzle.

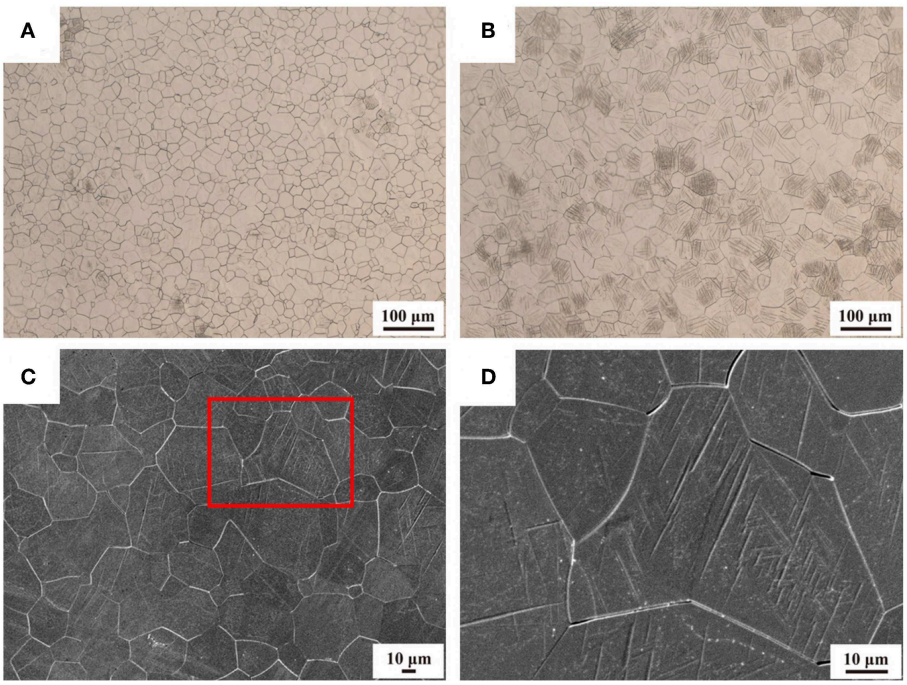

FIGURE 2 | Microstructure of Ti-35Nb-2Ta-3Zr alloy: **(A)** optical micrograph of the base metal, **(B)** optical micrograph of the laser-quenched alloy, **(C)** SEM of the laser-quenched alloy, **(D)** magnified SEM image of the rectangle in **(C)**.

RESULTS AND DISCUSSION

Microstructure and Phase Constitutions

Figure 2 shows the representative microstructure of the initial and laser-quenched Ti-35Nb-2Ta-3Zr alloy. The materials before and after laser quenching are equiaxed grains, indicating that the processing does not change the original morphology of the alloy. These images clearly reveal the grain coarsening and martensitic transformation during laser quenching. The diameter of the average grain evolved from 17.1 μm in the initial metal up to 30.3 μm (**Figures 2A,B**), because the β grains had grown severely under the action of short-time ultra-high temperature due to excessive scanning power and speed during the laser quenching. It can be seen from **Figures 2B–D** that acicular martensite α" martensite is present, which can be more clearly seen from the magnified SEM image (**Figure 2D**). This α′′ martensitic transformation was induced by laser quenching, which is not stress-induced martensite but heat-induced martensite. Martensitic transformation also occurred when laser remelting was performed on the surface of pure titanium of Sun et al. (2003), and it influenced the mechanical properties of the material.

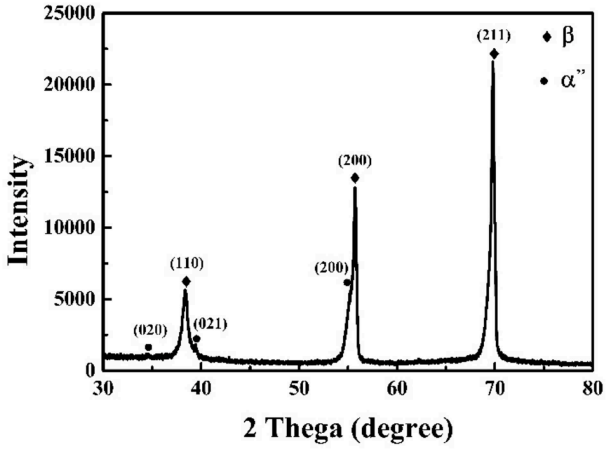

FIGURE 3 | XRD profile of the laser-quenched Ti-35Nb-2Ta-3Zr alloy.

Figure 3 is the X-ray diffraction pattern of the laser-quenched Ti-35Nb-2Ta-3Zr alloy. As can be seen from the profile, there are β phase peaks and α″ martensite peaks. Compared to the five or six martensites diffraction peaks during the cold rolling process (Guo et al., 2007; Wang et al., 2008a,c; Maghsoudlou et al., 2018), the number of martensite peak after laser quenching is very small. This may be the result of fast heating and cooling rates during laser quenching, which allow only a short time for phase transformations (Konstantino and Altus, 1999). The temperature of Ms (martensitic start) is lower than room temperature, and the martensite transformation is easy to induced with a small number of external stress in metastable β titanium alloys (Wang et al., 2009b; Min et al., 2012). Thus, when the alloy was deformed at room temperature (e.g., cold rolling), a higher critical sliding stress made martensite transformation easier. It reveals that β → α″ martensite phase transformation is more sensitive to stress than temperature.

TEM Analysis

To further analyze the microstructure and deformation behavior of the β-Ti-35Nb-2Ta-3Zr alloy after laser quenching, a transmission electron microscopy (TEM) was used to observe the surface of the laser-quenched zone. **Figure 4** shows the TEM and HRTEM micrographs of the sample in corresponding region. A weak strip-shaped α″ martensite phase with a size of about 16.7 nm appeared in **Figure 4A**, and the weak α″ phase peaks also appeared in the previous XRD profile (**Figure 3**), which again proved that β phase transforms to α″ martensite phase in the processing. In **Figure 4B**, significantly deformed microstructures and high-density dislocation tangles were found (as indicated by the white arrow). This phenomenon can be seen in many mechanical processes (Min et al., 2012; Lin et al., 2013; Liu et al., 2015; Wang et al., 2017; Lai et al., 2018; Maghsoudlou et al., 2018), and the dislocation tangles had a bad influence on phase transformation, leading to more martensite nucleation than martensite propagation. Therefore, the number of martensite detected is small, which should be due to the dislocation tangles. Moreover, because the material is subjected to internal stress, when the stress threshold is reached, the dislocation slip mechanism to be activated, resulting in the high-density dislocation tangles.

The corresponding selected area electron diffraction (SAED) (**Figure 4C**) revealed that the β phase and α″ martensite phase were obtained from the [111]β zone axis and the [110]α″ zone axis, respectively, and showed that the orientation relationship between α″ martensite and β matrix is [110]α″//[111]β. In the surface modification process of Ti-35Nb-2Ta-3Zr alloy by FSP, Lai et al. (2018) found that there are metastable zig-zag structured ω phase. It was mentioned that the introduction of high-density dislocation tangles contributes to hinder the formation of ω phase. In this paper, there is no ω phase appears in the **Figure 3** or **Figure 4**, which may be owing to a large number of dislocation tangles appeared in the laser-quenched alloy as shown in **Figures 4A,B**, so it can be concluded that the laser quenching cannot induce the ω phase transformation.

The atomic configurations of the β matrix had been examined by using high resolution TEM (HRTEM). **Figure 4D** is the HRTEM image seen from the [111]β axis of the β matrix, **Figure 4E** shows that the atomic spacing of the β matrix is measured about 0.277 nm. **Figure 4F** is the lattice distortion region of the HRTEM showing the irregular atomic arrangement. It should be noted that the surface is not flat at the atomic scale and some lattice fringes are not straight after laser quenching. This lattice distortion phenomenon also occurred when though eutectic reaction to prepare the layer-like NiTiNb porous metal due to the high density of stacking faults that twins have, and the dislocation activities may accelerate the lattice distortions during tensile deformation (Wang et al., 2018). In addition, this lattice distortion will occur during the martensitic transformation process. Therefore, heat-induced martensite transformation and dislocation activities are responsible for this phenomenon in this paper.

Microhardness Analysis

Along the laser-quenched surface of the Ti-35Nb-2Ta-3Zr sample (as shown by the black dotted line in **Figure 5B**), the microhardness distribution from the base metal to the laser-quenched zone as shown in **Figure 5A**. It can be clearly seen from the microhardness distribution curve of the laser-quenched Ti-35Nb-2Ta-3Zr alloy is uneven, the microhardness value of base metal is about 165 HV, and the microhardness value of quenching zone reach 181 HV, which increases by 9%. According to our knowledge, the increase in microhardness during laser quenching can be put down to two main factors. On the one hand, materials suffer from rapidly heat and cooling, β phase with lower hardness is transformed to highly hard and brittle martensite, resulting in microhardness increases (Sun et al., 2003). On the other hand, a lot of dislocations and lattice distortions are formed on the surface of samples leading to the surface hardening as shown in **Figures 4B,F**, so the microhardness increases. In the research (Wang et al., 2018), the refined grain size also helps to increase microhardness of the material, which due to the microhardness of polycrystalline materials increase with the decrease of grain size.

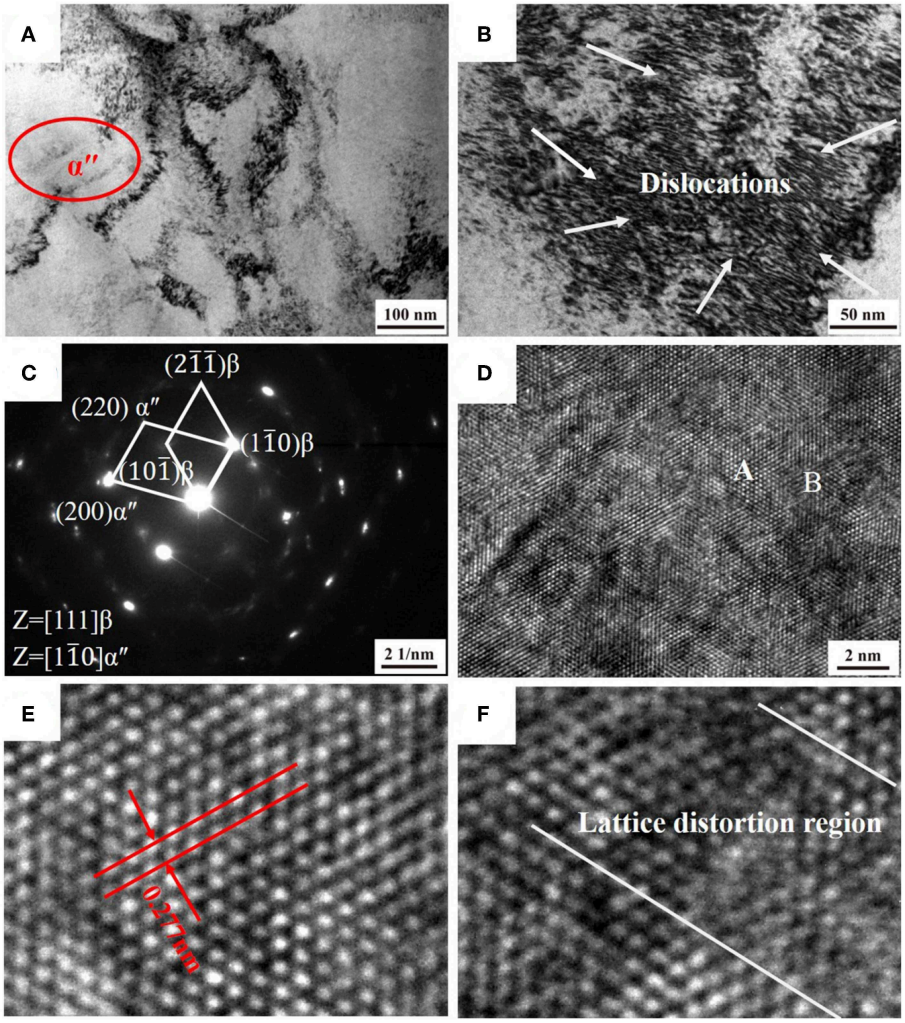

FIGURE 4 | TEM and HRTEM micrographs: **(A)** bright-field micrograph of laser-quenched Ti-35Nb-2Ta-3Zr alloy; **(B)** image of dislocation structure; **(C)** SAED patterns of **(A)**; **(D)** HRTEM image shown along the [111]β zone axis; **(E,F)** are magnified HRTEM figures of the region A and B in **(D)**, respectively.

However, as can be clearly seen from **Figure 2B** above, although the grain size increases significantly after laser quenching, the hardness of the quenching zone still increases (**Figure 5A**). It implied that the grain size has little effect on the microhardness, and dislocation activation and α″ martensite transformation are the main reasons for the increase in microhardness.

Superelastic Behavior

To expound the effect of laser quenching on the superelasticity of Ti-35Nb-2Ta-3Zr alloy, cyclic-tensile tests were conducted and the results were shown on **Figure 6**. The cyclic tensile strain for the alloys before and after laser quenching were 1, 2, 3, 4%. The superelastic features of laser-quenched specimens were described the residual strain (ε_R), the superelastic strain (ε_{SE}), and pure elastic strain (ε_E) during unloading (Wang et al., 2008b), respectively.

It can be observed from the stress-strain curves that the accumulation of residual strain on deformation (X axis). For the base and laser-quenched Ti-35Nb-2Ta-3Zr alloy (**Figures 6A,B**), residual strain can be seen in every cycle, indicating that irreversible plastic deformation occurred. The gradual accumulation of plastic deformation resulted in dislocation pile-up and tangles as shown in **Figure 4B**, which might hinder martensitic decomposition (Zhu et al., 2012). There are obvious non-linear deformation features appearing in **Figures 6A,B**, while much more non-linearity occurs in **Figure 6B**. Niinomi et al. (2008) investigated the non-linear elastic behavior of Ti–Nb–Ta–Zr system titanium alloy and stated that dislocation slip starts activating when the elastic strain attains to the lowest level belonging to a certain crystal direction. Therefore, the elastic modulus of the alloy is significantly decreased and the elastic behavior not obey Hooke's law. It is called superelasticity and is related to martensitic transformation. **Figure 6C** shows the superelastic recovery and elastic recovery strain of the two samples after unloading. The maximum ε_{SE} value for base metal is 0.38%

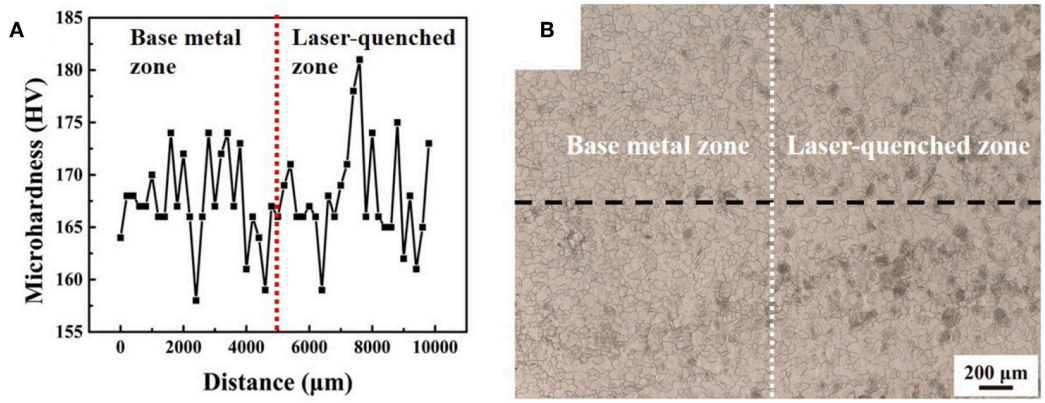

FIGURE 5 | (A) Microhardness of the Ti-35Nb-2Ta-3Zr alloy, **(B)** metallographic image of microhardness points positions.

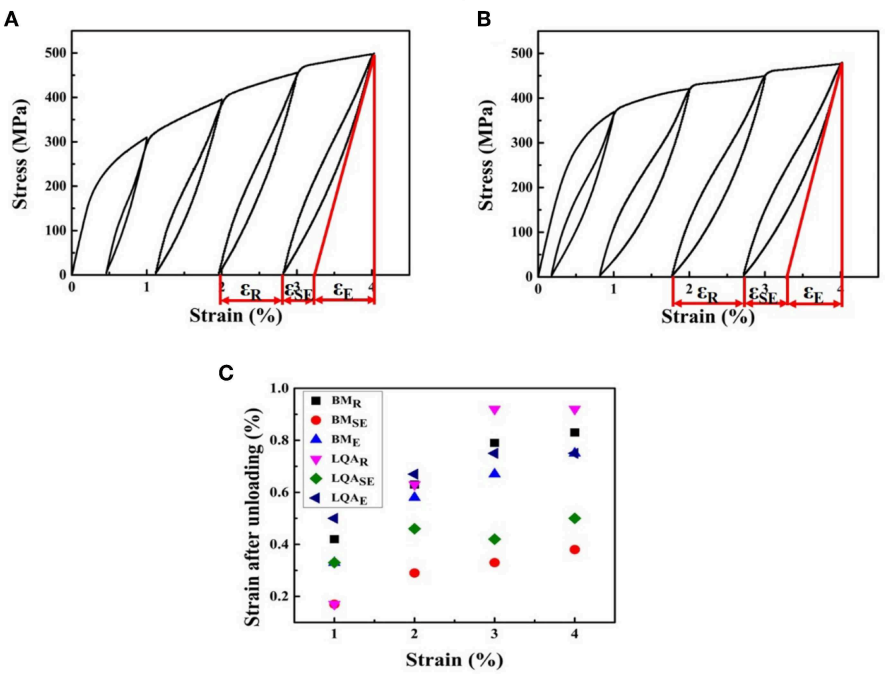

FIGURE 6 | Stress-strain curves of cyclic tensile tests of Ti-35Nb-2Ta-3Zr alloy: **(A)** base metal, **(B)** laser-quenched alloy, and **(C)** comparison of strain after unloading (BM, base metal; LQA, laser-quenched alloy).

when the tensile strain is 4%. For laser quenched alloy, the maximum value measured is about 0.5% at the same tensile strain during superelastic recovery. Compared to the base metal, with the increase in tensile strain, the ε_{SE} value is higher for laser-quenched alloy during superelastic recovery stage. The elastic recovery value can be intercepted by expanding the initial linear unloading stiffness [X] (strain) (Wang et al., 2018). The elastic recovery value can be intercepted from X axis (strain) by extending the original linear unloading stiffness (Wang et al., 2018). It can be observed that the elastic recovery strain for all samples is nearly 0.8% when the tensile strain is 4% during the elastic recovery stage. This superelastic behavior is attributed to more martensite transformation and reverse transformation occurring during cyclic tensile tests of the laser-quenched Ti-35Nb-2Ta-3Zr alloy.

α″ martensite transformation is very important in β-titanium alloys, which not only grants superelastic properties, but also accommodates both elastic and plastic strains (Maghsoudlou et al., 2018; Yang et al., 2018). In previous researches (Lai et al., 2018; Maghsoudlou et al., 2018), stress-induced martensitic transformation occurred in the early stage of plastic deformation of β titanium alloys, causing the yielding phenomenon. And

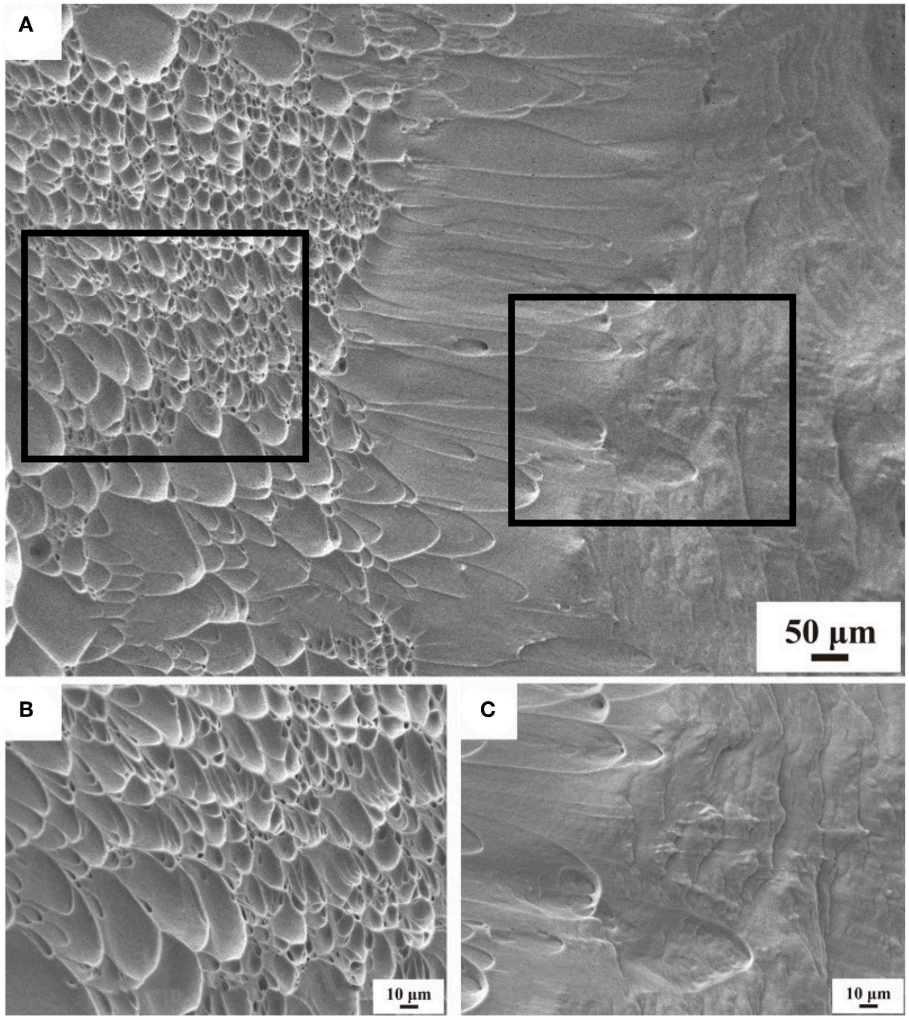

FIGURE 7 | The SEM fractographic images: **(A)** the laser-quenched Ti-35Nb-2Ta-3Zr alloy, **(B,C)** show high-magnification images taken from the black rectangle in **(A)**.

the yield strength value is equivalent to the critical stress value of the induced $\beta \rightarrow \alpha''$ martensite transformation. According to Lin et al. (2013) and Bingjie et al. (2018), the deformation behavior in β-titanium alloys was revealed by comparing the critical stress of dislocation slip (σ_{SDS}) and martensitic transformation (σ_{SIM}). If $\sigma_{SDS} < \sigma_{SIM}$, dislocation slip occurred before martensitic transformation are induced. After unloading, the condition ($\sigma_{SDS} < \sigma_{SIM}$) would have less strain recovery than the condition ($\sigma_{SDS} > \sigma_{SIM}$). In the present study, laser-quenched alloys (219 MPa) had higher yield strength than base metal (186 MPa). This is why the alloys after quenching has better superelasticity. In the study of Yang et al. (2018), the $\beta \rightarrow \alpha''$ martensite transformation also occurred first and then dislocations appeared. In addition, the small amount of martensite transformation should be the main reason for the slightly higher superelastic recovery performance after laser quenching.

Fracture Surfaces

Fracture surface of the laser-quenched Ti-35Nb-2Ta-3Zr alloy after tensile testing is shown in **Figure 7A**, which exhibits a complex fracture mode of dimple and cleavage. Plastic instabilities are the cause of the appearance of dimples characteristics, so the dimples features are used to indicate the level of plastic deformation (Rabadia et al., 2018; Zhang et al., 2018). The dimples in **Figure 7B** indicates a ductile fracture, and the cleavage plans in **Figure 7C** shows a brittle fracture. It can be seen from **Figure 7A** that the area of the cleavage plans (laser-quenched layer) is almost equal to the dimples regions (base metal), which indicates that toughness of the laser-quenched material is reduced and brittleness is increased. The main reason is that α'' martensite phase transformation occurs during laser scanning, and the martensite with higher brittleness, which leads to a decrease in material toughness. This is consistent with the results described above.

CONCLUSIONS

The microstructural evolution, mechanical properties, and deformation mechanisms of laser-quenched β-Ti-35Nb-2Ta-3Zr alloy were studied. Therefore, the key conclusions were drawn from this work are outlined below.

1) After laser quenching, grain coarsening and martensitic transformation occurred. The average grain size of the laser-quenched Ti-35Nb-2Ta-3Zr alloy increases from 17.1 μm in the initial metal to 30.3 μm.
2) Dislocations activated after martensitic transformation during the laser quenching process. β phase and α″ martensitic phase in the laser-quenched Ti-35Nb-2Ta-3Zr alloy was identified by transmission electron microscope (TEM) observation, and the orientation relationship between α″ martensite and β matrix is [110]α″//[111]β. It was also found in the XRD profile, and the content of α″ martensite is less than that of β phase.
3) The superelasticity of the laser-quenched Ti-35Nb-2Ta-3Zr alloy is slightly increased, which is due to the number of martensite transformation is less during laser quenching.
4) The laser-quenched Ti-35Nb-2Ta-3Zr alloy had a complex fracture mechanism including brittle fracture and toughness fracture, which was related to the transformation of the martensite phase.

DATA AVAILABILITY STATEMENT

All datasets generated for this study are included in the article/supplementary material.

AUTHOR CONTRIBUTIONS

TZ: organized and analyzed data and wrote the full manuscript. QF: analyzed data and wrote the part of the manuscript. XM: mainly responsible for doing experiments and providing experimental funds. WW, KW, PS, and JY: participated in modifying the manuscript.

FUNDING

The authors would like to acknowledge the financial support provided by the National Science Foundation under Grant Nos. 81828007, 51504152.

REFERENCES

Baker, T. N. (2010). 12 – laser surface modification of titanium alloys[J]. *Surface Surf. Engineering of. Light Alloys*. 398–443. doi: 10.1533/9781845699451.2.398

Bingjie, Z., Yuting, L., Yang, D., Liqiang, W., and Weijie, L., et al. (2018). The grain refinement mechanisms of various phases in shot-peened nickel-aluminum bronze (NAB) alloy[J]. *Mater. Charact.* 144, 77–85. doi: 10.1016/j.matchar.2018.07.002

Chen, H. T., Chung, C. J., Yang, T. C., Tang, C. H., and He, J. L. (2013). Microscopic observations of osteoblast growth on micro-arc oxidized β titanium[J]. *Appl. Surf. Sci.* 266, 73–80. doi: 10.1016/j.apsusc.2012.11.087

Chen, Z., Zhu, Q., Wang, J., Yun, X., He, B., and Luo, J. (2018). Behaviors of 40Cr steel treated by laser quenching on impact abrasive wear[J]. *Opt. Laser Technol.* 103, 118–125. doi: 10.1016/j.optlastec.2018.01.039

Chouirfa, H., Bouloussa, H., Migonney, V., and Falentin-Daudré, C. (2018). Review of titanium surface modification techniques and coatings for antibacterial applications[J]. *Acta Biomater.* 83, 37–54. doi: 10.1016/j.actbio.2018.10.036

Dai, Z. D., Pan, S. C., Wang, M., Yang, S. R., Zhang, X. S., and Xue, Q. J. (1997). Improving the fretting wear resistance of titanium alloy by laser beam quenching. *Wear* 213, 135–139. doi: 10.1016/S0043-1648(97)00160-9

Ding, Z., Fan, Q., and Wang, L. (2019). A review on Friction stir processing of titanium alloy: characterization, method, microstructure, properties[J]. *Metall. Mater. Trans. B* 50, 2134–2162. doi: 10.1007/s11663-019-01634-9

Ding, Z., Zhang, C., Xie, L., Zhang, L. C., Wang, L., and Lu, W. (2016). Effects of friction stir processing on the phase transformation and microstructure of TiO2-compounded Ti-6Al-4V Alloy[J]. *Metall. Mater. Trans. A*, 47, 5675–5679. doi: 10.1007/s11661-016-3809-8

Gao, J., Huang, Y., Guan, D., Knowles, A. J., Ma, L., Dye, D., et al. (2018). Deformation mechanisms in a metastable beta titanium twinning induced plasticity alloy with high yield strength and high strain hardening rate[J]. *Acta Mater.* 152, 301–314. doi: 10.1016/j.actamat.2018.04.035

Gao, J., Knowles, A. J., Guan, D., and Rainforth, W. M. (2019). ω phase strengthened 1.2 GPa metastable β titanium alloy with high ductility. *Scr. Mater.* 162, 77–81. doi: 10.1016/j.scriptamat.2018.10.043

Guo, B., Zhou, J., Zhang, S., Zhou, H., Pu, Y., and Chen, J. (2007). Phase composition and tribological properties of Ti–Al coatings produced on pure ti by laser cladding. *Appl. Surf. Sci.* 253, 9301–9310. doi: 10.1016/j.apsusc.2007.05.056

Konstantino, E., and Altus, E. (1999). Fatigue life enhancement by laser surface treatment[J]. *Surf. Eng.* 15, 126–128. doi: 10.1179/026708499101516461

Lai, M., Tasan, C. C., and Raabe, D. (2016). On the mechanism of {332} twinning in metastable β titanium alloys[J]. *Acta Mater.* 111, 173–186. doi: 10.1016/j.actamat.2016.03.040

Lai, M. J., Li, T., and Raabe, D. (2018). ω phase acts as a switch between dislocation channeling and joint twinning-and transformation-induced plasticity in a metastable β titanium alloy[J]. *Acta Mater.* 151, 67–77. doi: 10.1016/j.actamat.2018.03.053

Lin, Z., Wang, L., Xue, X., Lu, W., Qin, J., and Zhang, D. (2013). Microstructure evolution and mechanical properties of a Ti−35Nb−3Zr−2Ta biomedical alloy processed by equal channel angular pressing (ECAP). *Mater. Sci. Eng. C* 33, 4551–4561. doi: 10.1016/j.msec.2013.07.010

Liu, W., Cheng, M., Wahafu, T., Zhao, Y., Qin, H., Wang, J., et al. (2015). The *in vitro* and *in vivo* performance of a strontium-containing coating on the low-modulus Ti35Nb2Ta3Zr alloy formed by micro-arc oxidation[J]. *J. Mater. Sci. Mater. Med.* 26:203. doi: 10.1007/s10856-015-5533-0

Liu, X., Chu, P. K., and Ding, C. (2004). Surface modification of titanium, titanium alloys, and related materials for biomedical applications[J]. *Mater. Sci. Eng. R Rep.* 47, 49–121. doi: 10.1016/j.mser.2004.11.001

Maghsoudlou, A., Zarei-Hanzaki, A., Abedi, H. R., Barabi, A., Pilehva, F., Dietrich, D., et al. (2018). The room temperature tensile deformation behavior of thermomechanically processed β-metastable Ti-Nb-Ta-Zr bio-alloy: the role of deformation-induced martensite. *Mater. Sci. Eng. A* 738, 15–23. doi: 10.1016/j.msea.2018.09.038

Man, H., Zhang, S., Cheng, F., and Yue, T. M. (2001). Microstructure and formation mechanism of *in situ* synthesized TiC/Ti surface MMC on Ti-6Al-4V by laser cladding. *Scr. Mater.* 44, 2801–2807. doi: 10.1016/S1359-6462(01)00977-0

Min, X. H., Tsuzaki, K., Emura, S., and Tsuchiya, K. (2012). Heterogeneous twin formation and its effect on tensile properties in Ti–Mo based β titanium alloys. *Mater. Sci. Eng. A* 554, 53–60. doi: 10.1016/j.msea.2012.06.009

Niinomi, M., Akahori, T., and Nakai, M. (2008). *In situ* X-ray analysis of mechanism of nonlinear super elastic behavior of Ti–Nb–Ta–Zr system beta-type titanium alloy for biomedical applications[J]. *Mater. Sci. Eng. C*, 28, 406–413. doi: 10.1016/j.msec.2007.04.028

Ozan, S., Lin, J., Li, Y., and Wen, C. (2017). New Ti-Ta-Zr-Nb alloys with ultrahigh strength for potential orthopedic implant applications[J]. *J. Mech. Behav. Biomed. Mater.* 75, 119–127. doi: 10.1016/j.jmbbm.2017.07.011

Rabadia, C. D., Liu, Y. J., Jawed, S. F., Wang, L., Li, Y. H., Zhang, X. H., et al. (2018). Improved deformation behavior in Ti-Zr-Fe-Mn alloys comprising the C14 type Laves and β phases[J]. *Mater. Des*. 160, 1059–1070. doi: 10.1016/j.matdes.2018.10.049

Saito, T. (2003). Multifunctional alloys obtained via a dislocation-free plastic deformation mechanism[J]. *Science* 300, 464–467. doi: 10.1126/science.1081957

Saji, V. S., Choe, H. C., and Brantley, W. A. (2009). An electrochemical study on self-ordered nanoporous and nanotubular oxide on Ti−35Nb−5Ta−7Zr alloy for biomedical applications[J]. *Acta Biomater.* 5, 2303–2310. doi: 10.1016/j.actbio.2009.02.017

Sathish, S., Geetha, M., Aruna, S. T., Balaji, N., Rajam, K. S., Ashokamani, R. et al. (2011). Studies on plasma sprayed bi-layered ceramic coating on bio-medical Ti−13Nb−13Zr alloy. *Ceram. Int.* 37, 1333–1339. doi: 10.1016/j.ceramint.2010.12.012

Sun, Z., Annergren, I., and Pan, D. (2003). Effect of laser surface remelting on the corrosion behavior of commercially pure titanium sheet. *Mater. Sci. Eng. A* 345, 293–300. doi: 10.1016/S0921-5093(02)00477-X

Tobe, H., Kim, H. Y., Inamura, T., and Hosada, H. (2014). Origin of {332} twinning in metastable β-Ti alloys. *Acta Mater.* 64, 345–355. doi: 10.1016/j.actamat.2013.10.048

Vlcak, P., Fojt, J., Weiss, Z., Kopeček, J., and Perina, V. (2019). The effect of nitrogen saturation on the corrosion behaviour of Ti-35Nb-7Zr-5Ta beta titanium alloy nitrided by ion implantation. *Surf. Coat. Tech.* 358, 144–152. doi: 10.1016/j.surfcoat.2018.11.004

Wang, L., Lu, W., Qin, J., et al. (2008c). Change in microstructures and mechanical properties of biomedical Ti-Nb-Ta-Zr system alloy through cross-rolling. *Mater. trans.* 49, 1791–1795. doi: 10.2320/matertrans.MRA2008040

Wang, L., Lu, W., Qin, J., Zhang, F., and Zhang, D. (2008a). Microstructure and mechanical properties of cold-rolled TiNbTaZr biomedical β titanium alloy. *Mater. Sci. Eng. A* 490, 421–426. doi: 10.1016/j.msea.2008.03.003

Wang, L., Lu, W., Qin, J., Zhang, F., and Zhang, D. (2008b). Texture and superelastic behavior of cold-rolled TiNbTaZr alloy. *Mater. Sci. Eng. A* 491, 372–377. doi: 10.1016/j.msea.2008.04.018

Wang, L., Lu, W., Qin, J., Zhang, F., and Zhang, D. (2009a). Effect of precipitation phase on microstructure and superelasticity of cold-rolled beta titanium alloy during heat treatment. *Mater. Des.* 30, 3873–3878. doi: 10.1016/j.matdes.2009.03.042

Wang, L., Lu, W., Qin, J., Zhang, F., and Zhang, D. (2009b). Influence of cold deformation on martensite transformation and mechanical properties of Ti–Nb–Ta–Zr alloy. *J. Alloys Compd.* 469, 512–518. doi: 10.1016/j.jallcom.2008.02.032

Wang, L., Qu, J., Chen, L., Meng, Q., Zhang, L. C., Qin, J., et al. (2015). Investigation of deformation mechanisms in β-Type Ti-35Nb-2Ta-3Zr Alloy via FSP leading to surface strengthening. *Metall. Mater. Trans. A* 46, 4813–4818. doi: 10.1007/s11661-015-3089-8

Wang, L., Xie, L., Lv, Y., Zhang, L. C., Chen, L., Meng, Q., et al. (2017). Microstructure evolution and superelastic behavior in Ti-35Nb-2Ta-3Zr alloy processed by friction stir processing. *Acta Mater.* 131, 499–510. doi: 10.1016/j.actamat.2017.03.079

Wang, L., Xie, L., Zhang, L. C., Chen, L., Ding, Z., Lv, Y., et al. (2018). Microstructure evolution and superelasticity of layer-like NiTiNb porous metal prepared by eutectic reaction. *Acta Mater.* 143, 214–226. doi: 10.1016/j.actamat.2017.10.021

Xie, L., Wen, Y., Zhan, K., Wang, L., Jiang, C., and Ji, V. (2016). Characterization on surface mechanical properties of Ti−6Al−4V after shot peening. *J. Alloys Compd.* 666, 65–70. doi: 10.1016/j.jallcom.2016.01.119

Yang, Y., Castany, P., Bertrand, E., Zhang, F., and Zhang, D. (2018). Stress release-induced interfacial twin boundary ω phase formation in a β type Ti-based single crystal displaying stress-induced α" martensitic transformation. *Acta Mater.* 149, 97–107. doi: 10.1016/j.actamat.2018.02.036

Yao, T., Du, K., Wang, H., et al. (2017). *In situ* scanning and transmission electron microscopy investigation on plastic deformation in a metastable beta titanium alloy. *Acta Mater.* 133, 21-−29. doi: 10.1016/j.actamat.2017.05.018

Zhang, L. C., and Chen, L. Y. (2019). A Review on biomedical titanium alloys: recent progress and prospect. *Adv. Eng. Mater.* 21:1801215. doi: 10.1002/adem.201801215

Zhang, L. C., Liu, Y., Li, S., and Hao, Y. (2018). Additive manufacturing of titanium alloys by electron beam melting: a review. *Adv. Eng. Mater.* 20:1700842. doi: 10.1002/adem.201700842

Zhu, Y., Wang, L., Wang, M., Huang, Z., Li, C., Li, L., et al. (2012). Superelastic and shape memory properties of Ti x Nb3Zr2Ta alloys. *J. Mech. Behav. Biomed. Mater.* 12, 151–159. doi: 10.1016/j.jmbbm.2012.02.010

Conflict of Interest: The authors declare that the research was conducted in the absence of any commercial or financial relationships that could be construed as a potential conflict of interest.